European Radiology

MAGNETIC RESONANCE Open Access

Non-invasive PD-L1 stratification in non-small cell lung cancer using dynamic contrast-enhanced MRI

Gaia Messana[1], Chandra Bortolotto[1,2], Sithin Thulasi Seetha[1,3*], Alessandra Marrocco[1], Carlotta Pairazzi[1], Francesco Sanvito[4,5], Francesca Brero[6,7], Agnese Robustelli Test[6,7], Raffaella Fiamma Cabini[8], Alessandro Lascialfari[6,7], Domenico Zacà[9], Giulia Maria Stella[10,11], Francesco Agustoni[12], Jessica Saddi[13], Andrea Riccardo Filippi[1,13,14,15] and Lorenzo Preda[1,2]

Abstract

Objectives This study aimed to assess whether pharmacokinetic parameters derived from DCE-MRI can stratify Programmed Death-Ligand 1 (PD-L1) expression in NSCLC. The secondary aim was to identify a suitable pharmacokinetic model configuration for anisotropic temporally-spaced DCE-MRI sequences, considering Tofts variants, population-averaged arterial input functions (AIF), and bolus arrival time (BAT) estimation methods.

Materials and methods From April 2021 to May 2023, patients with locally advanced non-small cell lung cancer (NSCLC) were prospectively enrolled. Tumors were categorized based on: PD-L1 absence/presence (threshold 1%) and hyperexpression/hypoexpression (threshold 50%). Pharmacokinetic parameters were extracted using several candidate configurations; fit quality was evaluated using coefficient of determination (R^2). Mann–Whitney U-test and ROC-AUC were used to assess correlation with PD-L1 for the best-fit configuration.

Results Thirty-eight patients (mean age 68 ± 9 years, 28 men) were included. PD-L1 expression was present in 25 patients (66%) and absent in 13 (34%). PD-L1 was hyperexpressed in 13 (34%) patients and hypoexpressed in 25 (66%). Voxel-wise pharmacokinetic parameters were extracted using the best-fit configuration—extended Tofts model (ETM) with Georgiou AIF and Peak-Gradient (PG) BAT estimation ($R^2 = 0.79$). K^{trans} median (0.25 vs. 0.12 min^{-1}, $p = 0.02$), K^{trans} standard deviation (0.32 vs. 0.23 min^{-1}, $p = 0.01$) and K_{ep} median (1.09 vs. 0.59 min^{-1}, $p = 0.02$) were significantly higher in PD-L1 < 50% group (ROC-AUC 0.71–0.76).

Conclusion DCE-MRI pharmacokinetic parameters could stratify PD-L1 hypo/hyperexpression in NSCLC. The ETM with PG BAT estimation method and Georgiou AIF was the best-performing pharmacokinetic configuration.

Key Points

Question *Could Dynamic Contrast-Enhanced (DCE) MRI offer a safe and non-invasive way to assess Programmed Death-Ligand 1 (PD-L1) expression?*

Findings *Quantitative DCE-MRI parameters K^{trans}* (the volume transfer rate) and K_{ep} (the efflux rate constant) show potential for distinguishing PD-L1 hyperexpression from hypoexpression.

Clinical relevance *Preliminary results suggest that DCE-MRI could be a safe method to stratify PD-L1 hypo/hyperexpression in non-small cell lung cancer, potentially optimizing treatment decisions, given the high cost of immunotherapy.*

Gaia Messana and Sithin Thulasi Seetha contributed equally to this work.

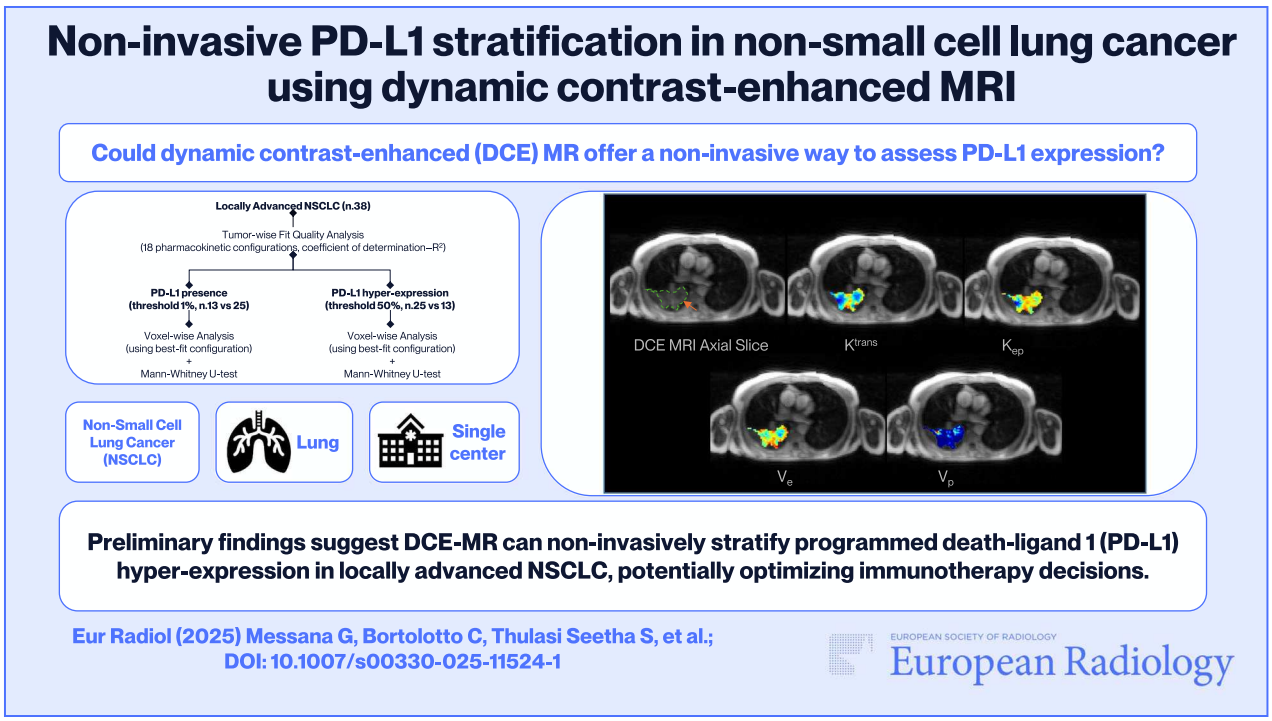
*Correspondence:
Sithin Thulasi Seetha
sithin.thulasiseetha@unipv.it
Full list of author information is available at the end of the article

Springer

© The Author(s) 2025. **Open Access** This article is licensed under a Creative Commons Attribution 4.0 International License, which permits use, sharing, adaptation, distribution and reproduction in any medium or format, as long as you give appropriate credit to the original author(s) and the source, provide a link to the Creative Commons licence, and indicate if changes were made. The images or other third party material in this article are included in the article's Creative Commons licence, unless indicated otherwise in a credit line to the material. If material is not included in the article's Creative Commons licence and your intended use is not permitted by statutory regulation or exceeds the permitted use, you will need to obtain permission directly from the copyright holder. To view a copy of this licence, visit http://creativecommons.org/licenses/by/4.0/.

Keywords Non-small cell lung carcinoma, Immunotherapy, PD-L1 inhibitors, Perfusion magnetic resonance imaging, Pharmacokinetics

Graphical Abstract



Introduction

Lung cancer is the most prevalent cancer globally and the leading cause of cancer-related deaths worldwide [1]. Non-small cell lung cancer (NSCLC) accounts for nearly 85% of all lung cancer cases. In NSCLC, immune checkpoint inhibitors (ICIs) targeting programmed cell death protein 1 (PD-1) or its ligand (PD-L1) have shown greater efficacy and lower toxicity compared to chemotherapy [2–4]. However, only 20–50% of patients achieve long-term positive treatment responses [5, 6]. This highlights the importance of accurate patient stratification before administering ICIs, to optimize therapeutic outcomes. The National Comprehensive Cancer Network (NCCN) currently recommends stratifying patients with NSCLC for immunotherapy based on PD-L1 expression, determined through tumor proportion score (TPS) via immunohistochemical (IHC) analysis on pathological samples [7]. For example, the main indications for the treatment with Pembrolizumab, a PD-L1 inhibitor, are: (1) as a first-line therapy for metastatic NSCLC with PD-L1 TPS ≥ 50% and (2) treatment for patients with metastatic NSCLC whose tumors express PD-L1 (TPS ≥ 1%), with disease progression or after chemotherapy [8]. Besides, numerous clinical trials have demonstrated the predictive value of PD-L1 TPS for treatment response [4, 9].

However, bioptic procedures carry significant risks and may not represent the overall PD-L1 status of the tumor [10]. Therefore, non-invasive, safer, and repeatable alternative methods to assess PD-L1 expression are needed.

In recent years, Dynamic Contrast-Enhanced MRI (DCE-MRI) has gained significant interest due to its potential to extract biological characteristics of tumors. DCE-MRI provides information on tumor microvascular properties, such as perfusion and permeability, and it has been applied in many cancer types, including breast, head and neck, and gastric tumors [11–14].

Lung MRI has historically been challenging due to the intrinsic properties of the organ, such as low proton density and movement artifacts. However, recent advancements in MRI sequences, such as improved gradient performance and free-breathing acquisitions, have increased interest in lung MRI. To our knowledge, no studies have examined the correlation between DCE-MRI pharmacokinetic parameters and PD-L1 expression in NSCLC.

The primary aim of this study was to investigate whether DCE-MRI pharmacokinetic parameters can stratify PD-L1 expression in NSCLC. The secondary aim was to identify the best configuration of the pharmacokinetic model for the DCE-MRI sequences designed for fast acquisition with anisotropic temporal resolution.

Materials and methods

Patient data

The study was conducted following the Declaration of Helsinki and approved by the Institutional Ethics Committee of Fondazione IRCCS Policlinico San Matteo. Informed consent was obtained from all subjects involved in the study.

From April 2021 to May 2023, we prospectively enrolled a consecutive cohort comprising patients diagnosed with locally advanced NSCLC (according to TNM classification VIII edition, stage III A-C, and T ≥ 2). Exclusion criteria were: (1) insufficient compliance to ensure completion of the MR examination; (2) any treatment before undergoing MRI; (3) absence of PD-L1 expression test. PD-L1 expression was quantified through the 22C3 pharmDx assay (Agilent Technologies) [15] and TPS was evaluated according to guidelines [16]. Tumors were categorized based on—(1) the presence/absence of PD-L1 expression (TPS ≥ 1% and TPS < 1%) and (2) PD-L1 hyperexpression/hypoexpression (TPS ≥ 50% and TPS < 50%).

MRI acquisition protocol

MRI was performed using a 1.5-Tesla scanner (MAGNETOM Aera; Siemens Healthcare) using an 18-channel surface coil. Scan sequences included volumetric interpolated breath-hold examination (VIBE) T1 sequences and free-breathing DCE sequences. The DCE-MR acquisition (Table 1) was based on time-resolved angiography with interleaved stochastic trajectories (TWIST). A bolus of gadoteric meglumine (Dotarem), at a clinical standard dose of 0.2 mL/kg, was injected intravenously at a rate of 3–4 mL/s (Fig. 1).

Table 1 Main features of dynamic contrast-enhanced MRI (DCE-MRI) sequence

DCE-MRI acquisition parameters	
Feature	**Value [median; interquartile range]**
Matrix	128 × 128
Repetition time (TR)	2.24–2.27 ms [2.25; 0.01]
Time to echo (TE)	0.73–0.74 ms [0.74; 0.01]
Field of view (FOV)	384–400 mm [400; 0.0]
Slice spacing	3 mm
Pixel-spacing	3.00–3.12 mm [3.12; 0.0]
Number of layers	30
Temporal resolution	1.33–84.23 s [1.34; 0.0]
Flip angle	23–25° [25; 0.0]
Number of measurements	30
Duration	0.8–3.48 min [1.47; 0.07]

Image preprocessing and segmentation

To reduce motion errors due to respiration and cardiac movement, we employed SimpleITK's diffeomorphic demons registration filter [17]. Tumor delineation was performed semi-automatically. Initially, an experienced radiologist segmented the tumor on pre-contrast VIBE images using ITK-SNAP software (http://www.itksnap.org). The segmentation mask was then aligned with the DCE-MRI series using SimpleITK's non-rigid BSpline registration technique, and any errors were manually corrected.

Arterial input functions

We explored three popular population arterial input functions (AIFs) proposed by Weinmann, Parker, and Georgiou. Each has a parameterized functional form, formulated by aggregating subject-wise AIFs extracted from DCE-MRI acquired with high temporal resolution [18–20] (Supplementary material (SM), section S1).

Bolus arrival time estimation

Bolus arrival time (BAT, t_0) estimation was incorporated into the pharmacokinetic model to enhance the fit. To ensure stability, BAT was initialized using automated BAT estimation methods applied to the tumor-derived mean time-signal intensity curve (TIC). Three commonly used methods were evaluated: Linear-Linear (LL), Linear-Quadratic (LQ), and Peak-Gradient (PG) (Fig. 2) (SM, section S2).

Pharmacokinetic modeling

We investigated two widely used variations of the Tofts bicompartmental model—the standard Tofts model (TM) and extended Tofts model (ETM)—to characterize tumor microvascular properties. Pharmacokinetic parameters, including K^{trans} (the volume transfer rate), K_{ep} (the efflux rate constant), V_e (the extracellular extravascular fraction), and V_p (the blood plasma volume fraction, only present in ETM), were optimized to fit the time-concentration curves (TCCs) using the Trust Region Reflective algorithm [21]. The steps involved in voxel-wise (tumor-wise) pharmacokinetic modeling can be summarized as follows: (1) Convert voxel-wise (mean-tumor) TIC to voxel-wise (mean-tumor) TCC; (2) Optimize the model parameters to fit the measured voxel-wise (mean-tumor) TCC; (3) For voxel-wise analysis, further compute the median, 90th percentile and standard deviation (SD) of non-necrotic voxels present within the target lesion; (4) Perform statistical (fit quality) analysis (SM, section S3).

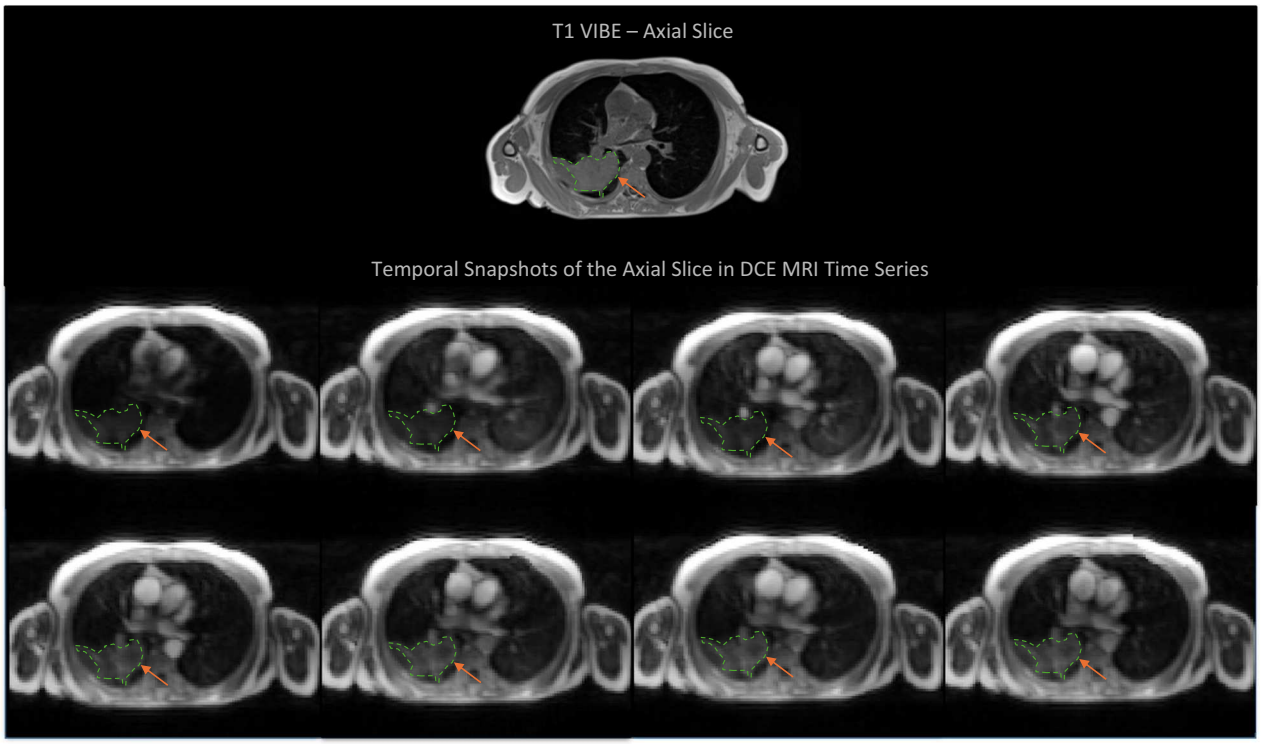


Fig. 1 Eight out of 30 images illustrating dynamic vascular changes over time for a sample non-breath-hold TWIST DCE-MRI time series. Annotations highlight the tumor. T1 VIBE axial slice has been included as a reference to illustrate tumor morphology

Fit quality analysis

To identify the best pharmacokinetic modeling approach for temporally anisotropic sequences, we investigated popular choices in three different levels of Tofts model design using mean-tumor TIC: (1) Tofts variants—standard or extended, (2) input population AIF—Weinmann, Parker, or Georgiou, and (3) BAT estimation methods—LL, LQ, or PG, collectively constituting 18 different configurations.

To quantify fit quality, we used the coefficient of determination, R^2. By excluding voxels with $R^2 \leq 0$, we eliminated the impact of necrotic or outlier (poor fit) voxels within the tumor.

Inter-reader agreement

First-order pharmacokinetic parameters extracted from tumor voxels may be subjected to variations due to changes in tumor delineation. To address this, we conducted an inter-reader agreement analysis on a random sample of ten patients. A second experienced radiologist independently performed manual segmentations on DCE-MR images. The agreement was assessed using the concordance correlation coefficient (CCC), with features having CCC > 0.85 classified as highly reproducible.

Statistical analysis

We performed a Kruskal-Wallis H-test to assess whether the extracted first-order pharmacokinetic features differ significantly between subgroups of tumor histologies. Mann–Whitney U-test was performed to check for significance in differences between the groups of PD-L1 absence/presence (PD-L1 thresholded at 1%) and hyper-expression/hypoexpression (PD-L1 thresholded at 50%). A p-value < 0.05 was considered statistically significant. The receiver operating characteristics area under the curve (ROC-AUC) was estimated to assess the discriminative performance. Python (v3.7.5) and SciPy packages were used for all statistical analysis. The Python-based implementation is provided as open-source and is available at https://github.com/sithin-unipv/lungmr_pk.git (accessed on 25/09/24).

Confounding factors analysis

To evaluate the potential impact of histology and nodal status as confounders on the statistically significant pharmacokinetic parameters, we conducted a bivariable analysis using logistic regression, adjusted for nodal status and histology.

Results

A total of 38 patients were included. Among them, 28 (74%) were males and 10 (26%) were females. All the

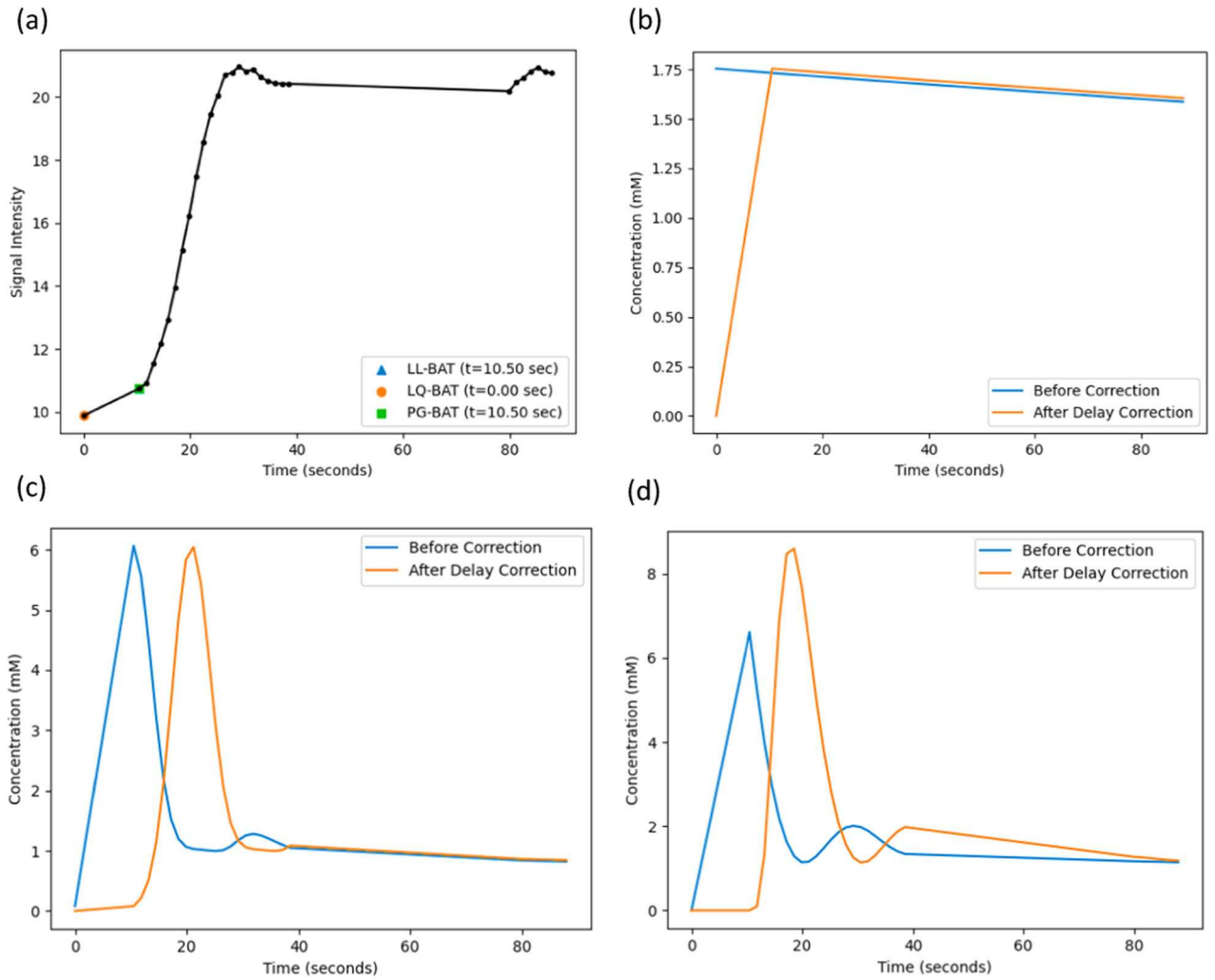


Fig. 2 **a** Comparison of the three different bolus arrival time (BAT) estimation methods—LinearLinear (LL), LinearQuadratic (LQ) and PeakGradient (PG) on the mean tumor signal for a sample patient; Subsequent visualization of delay corrected population arterial input functions—**b** Weinmann, **c** Parker, and **d** Georgiou. For visualizing delay correction, we used the BAT estimated using the PG method

patients were of Caucasian ethnicity, with an average age of 68 ± 9 years. There were 14 patients (36%) with lung adenocarcinoma, 12 (32%) with lung squamocellular carcinoma, and 12 patients (32%) with poorly differentiated NSCLC. Of these, 25 (66%) had a PD-L1 expression (≥ 1%), and 13 (34%) showed PD-L1 hyperexpression (≥ 50%). Table 2 summarizes the main patient characteristics.

Pharmacokinetic parameters—K^{trans}, K_{ep}, V_e, and V_p (only for ETM) were estimated by fitting 18 distinct model configurations on the mean-tumor TIC. The median R^2 values ranged from 0.06 to 0.79 (Table 3). The ETM pharmacokinetic model with Georgiou AIF and PG BAT estimation method was the best-performing configuration, resulting in a median R^2 of 0.79. This configuration was later used to extract ETM parametric maps.

Kruskal-Wallis H-test showed no statistically significant differences ($p > 0.05$) among first-order pharmacokinetic features derived from the parametric maps across tumor histologies (Table S1). Inter-reader agreement analysis revealed that the features median (K^{trans}), median (K_{ep}), median (V_e), 90th percentile (V_e), and SD (V_e) were highly reproducible (CCC: 0.90–0.96) (Table S2).

For the 50% threshold of PD-L1 expression, there were significant differences in features extracted from the K^{trans} and K_{ep} maps. For K^{trans}, higher values were observed in the hypoexpression PD-L1 group for the features: median (0.25 vs. 0.12 min^{-1}, $p = 0.02$), 90th percentile (0.74 vs. 0.44 min^{-1}, $p = 0.01$), and SD (0.32 vs. 0.23 min^{-1}, $p = 0.01$). Similarly, for K_{ep}, higher values were observed in the hypoexpression PD-L1 group for the features:

Table 2 Summary of patients' characteristics

Main patient characteristics ($n = 38$)	
Characteristic	**Value**
Age (years)	
Median	68
Range	50–85
Sex	
Female	26% (10)
Male	74% (28)
Histology	
Adenocarcinoma	36% (14)
Squamous cell carcinoma	32% (12)
NSCLC poorly differentiated	32% (12)
Nodal Status	
N0 (negative)	11% (4)
N1-N3 (positive)	89% (34)
PD-L1 expression	
PD-L1 ≥ 1%	66% (25)
PD-L1 < 1%	34% (13)
PD-L1 hyperexpression/hypoexpression	
PD-L1 ≥ 50%	34% (13)
PD-L1 < 50%	66% (25)

Table 3 Results of the fit quality analysis for the 18 different configurations examined on the mean tumor contrast agent concentration curve

PK model	AIF	BAT	Median R^2
Extended Tofts	Georgiou	LL	0.694
		LQ	0.653
		PG	0.789
	Parker	LL	0.702
		LQ	0.682
		PG	0.788
	Weinmann	LL	0.546
		LQ	0.454
		PG	0.527
Standard Tofts	Georgiou	LL	0.709
		LQ	0.660
		PG	0.765
	Parker	LL	0.679
		LQ	0.671
		PG	0.682
	Weinmann	LL	0.221
		LQ	0.303
		PG	0.065

PK pharmacokinetic, *AIF* arterial input function, *BAT* bolus arrival time, R^2 coefficient of determination, *LL* linear-linear, *LQ* linear-quadratic, *PG* peak-gradient

median (1.09 vs. 0.59 min^{-1}, $p = 0.02$) and 90th percentile (2.21 vs. 1.87 min^{-1}, $p = 0.04$) (Table 4).

Mann–Whitney U-tests for the 1% threshold revealed no statistical significance ($p > 0.05$) (Table 5). Figure 3 illustrates the distribution and ROC-AUC of the significant features identified in this study. Figure 4 presents the parametric maps extracted for a sample lesion. Of note, the ETM parameters estimated using the mean tumor TIC were close to the median parameter map estimates (Table S3).

The bivariable logistic regression analysis on clinically significant features revealed that median(K_{ep}), median(K^{trans}), and SD(K^{trans}) are independent predictors ($p < 0.05$), unaffected by histology or nodal status (Table S4).

Discussion

In this study, we utilized short-period temporally anisotropic lung DCE-MRI sequences of NSCLC patients to investigate the role of pharmacokinetic parameters in the stratification of PD-L1 expression. Furthermore, we identified a suitable pharmacokinetic configuration for this custom sequence, in terms of choices in Tofts model type, BAT estimation method, and population AIF. We categorized patients according to two PD-L1 TPS thresholds: (1) PD-L1 ≥ 1%, reflecting the clinical eligibility criteria for immunotherapy, and (2) PD-L1 ≥ 50%, commonly used to identify patients with high PD-L1 expression who are more likely to benefit from immunotherapy. Our results demonstrated a negative correlation between K^{trans} and K_{ep} values with PD-L1 expression and showed moderate accuracy in discriminating PD-L1 hyperexpression. ETM with PG BAT estimation method and Georgiou AIF was the best-performing pharmacokinetic configuration.

DCE-MRI may be leveraged to quantify perfusion and microvascular parameters by fitting pharmacokinetic models to contrast concentration curves [22]. The principal quantitative parameters obtained from ETM are: K^{trans}, the volume transfer constant of contrast agent leaked into extravascular extracellular space (EES) from plasma; K_{ep}, the rate constant of contrast agent reflux to the plasma; V_e, the EES volume fraction; and V_p, the plasma volume fraction [23]. As vascular abnormality is one of the primary features of malignant tumors, DCE-MRI has been extensively evaluated to extrapolate the pharmacokinetic parameters associated with these diseases [24]. Nonetheless, there is a relatively low number of publications on the application of DCE-MRI to lung tumors due to its limited use in clinical practice and the technical challenges of lung MRI.

In the study of Wang et al elevated K^{trans} values correlated positively with better treatment response leading to extended progression-free survival (PFS) and overall

Table 4 Results for the 50% threshold of PD-L1 expression

Feature	Median (PD-L1 < 50%)	Median (PD-L1 ≥ 50%)	ROC-AUC	95% CI	Threshold	Acc	Sensitivity/Specificity	*p*-value
Median (K_{ep})	**1.089879**	**0.590350**	**0.729**	**[0.56, 0.88]**	**0.95**	**0.68**	**0.64/0.85**	**0.022791**
90th percentile (K_{ep})	**2.213419**	**1.875468**	**0.711**	**[0.53, 0.86]**	**2.78**	**0.63**	**0.48/0.92**	**0.036411**
Standard deviation (K_{ep})	1.347053	1.147729	0.594	[0.41, 0.78]	1.30	0.63	0.60/0.77	0.355967
Median (K^{trans})	**0.246861**	**0.120352**	**0.735**	**[0.56, 0.89]**	**0.18**	**0.68**	**0.68/0.77**	**0.019363**
90th percentile (K^{trans})	**0.740485**	**0.436491**	**0.726**	**[0.55, 0.88]**	**0.55**	**0.74**	**0.76/0.69**	**0.024694**
Standard deviation (K^{trans})	**0.321472**	**0.232454**	**0.757**	**[0.58, 0.90]**	**0.30**	**0.68**	**0.68/0.77**	**0.010654**
Median (V_e)	0.243500	0.215956	0.585	[0.40, 0.76]	0.28	0.53	0.36/0.92	0.406104
90th percentile (V_e)	0.414260	0.398898	0.572	[0.38, 0.75]	0.53	0.50	0.24/1.00	0.479136
Standard deviation (V_e)	0.127310	0.119866	0.535	[0.34, 0.73]	0.12	0.58	0.64/0.54	0.735015
Median (V_p)	0.008537	0.008100	0.526	[0.33, 0.73]	0.00	0.66	0.80/0.38	0.805563
90th percentile (V_p)	0.049675	0.032970	0.609	[0.41, 0.79]	0.05	0.58	0.52/0.77	0.281515
Standard deviation (V_p)	0.032906	0.024364	0.612	[0.41, 0.80]	0.03	0.58	0.72/0.62	0.267995

PD-L1 programmed death ligand 1, *ROC-AUC* area under the receiver operating characteristic curve, *95% CI* 95% confidence interval of ROC-AUC, *Acc* accuracy
Statistically significant PK parameters' rows ($p < 0.05$) are highlighted

survival (OS) in unresectable stage III NSCLC patients who underwent immunotherapy [25]; Sridharan et al showed that K^{trans} is repeatable and detects early treatment-induced changes in NSCLC lesions, supporting its use in the evaluation of biological response to radiotherapy and targeted therapies [26]. Regarding histological differentiation, Guo et al identified K^{trans} as a promising parameter to differentiate small-cell lung cancer from NSCLC and adenocarcinoma from squamous cell carcinoma [27]. Zou et al demonstrated that some K^{trans} and K_{ep} features were reliable in evaluating the epidermal growth factor receptor (EGFR) gene mutation status and the expression of vascular endothelial growth factor (VEGF) and EGFR proteins in NSCLC [28]. No previous studies have explored the correlation between DCE-MRI parameters and PD-L1 expression in lung cancer.

Our results showed significantly higher K_{ep} and K^{trans} values in patients with PD-L1 TPS < 50% compared to the group with PD-L1 TPS ≥ 50%, with moderate diagnostic accuracy, while being independent of confounding factors like histology and nodal status. NSCLC, like many other tumors, is characterized by the upregulation of pro-angiogenic factors. This results in the formation of an aberrant vascular network with increased vessel permeability, due to defective endothelial cell junctions and the overproduction of permeability-inducing agents such as VEGF [29, 30]. K^{trans} is a parameter that combines blood flow and permeability, and it has been shown to reflect blood flow under conditions of very high permeability, such as those found in tumors [31]; moreover, in this cohort of patients, the use of gadoteric acid, a lipophilic contrast agent that easily crosses the endothelial wall, further increases permeability [32]. K_{ep} is associated with microvessel density, and both K^{trans} and K_{ep} parameters can reflect tumor proliferation potential [33, 34]. Therefore, our results suggest that tumors with PD-L1 hyperexpression may have lower blood flow and reduced microvessel density compared to tumors with lower PD-L1 expression. This finding is in line with the study by Bortolotto et al [35], which reported an inverse correlation between D* values—representing the perfusion-related diffusion coefficient in intravoxel incoherent motion diffusion-weighted imaging (IVIM-DWI) and PD-L1 expression [35]. Also, our results are consistent with those of Franz et al who demonstrated a negative correlation between angiogenesis (marked by CD31) and PD-L1 expression in laryngeal carcinomas [36]. A possible explanation is that the greater infiltration of immune cells, likely present in tumors with higher PD-L1 expression [37], is associated with increased vessel permeability, leading to blood stasis and reduced blood flow in the local microcirculation. However, pharmacokinetic models

Table 5 Results for the 1% threshold of PD-L1 expression

Feature	Median (PD-L1 < 1%)	Median (PD-L1 ≥ 1%)	ROC-AUC	*p*-value
Median (K_{ep})	0.973981	0.849796	0.507	0.950930
90th percentile (K_{ep})	2.007770	2.132588	0.545	0.666636
Standard deviation (K_{ep})	1.224932	1.240920	0.483	0.877731
Median (K^{trans})	0.246861	0.175889	0.523	0.829467
90th percentile (K^{trans})	0.693362	0.605147	0.535	0.735015
Standard deviation (K^{trans})	0.302964	0.298183	0.569	0.498455
Median (V_e)	0.232556	0.238432	0.489	0.926454
90th percentile (V_e)	0.413462	0.411794	0.501	1.000000
Standard deviation (V_e)	0.120894	0.123767	0.486	0.902046
Median (V_p)	0.008042	0.008537	0.529	0.781839
90th percentile (V_p)	0.033862	0.045000	0.502	1.000000
Standard deviation (V_p)	0.027926	0.036257	0.489	0.926454

PD-L1 programmed death ligand 1, *ROC-AUC* area under the receiver operating characteristic curve

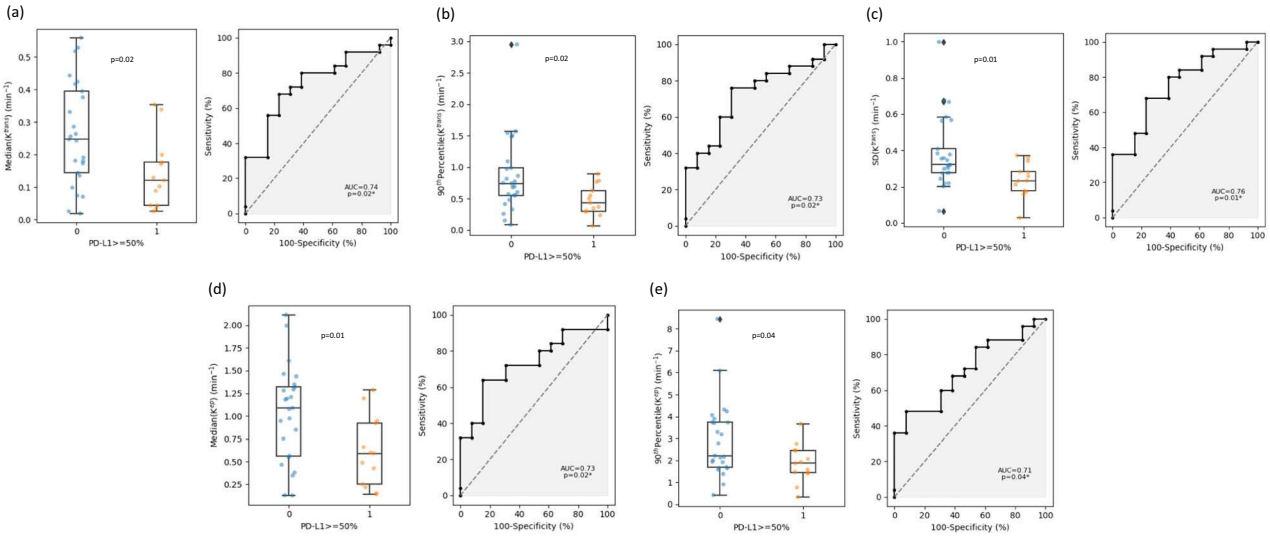


Fig. 3 The distribution plot and ROC curves of statistically significant pharmacokinetic parameters identified in this study: **a** Median (K^{trans}); **b** 90th percentile (K^{trans}); **c** Standard deviation, SD (K^{trans}); **d** Median (K_{ep}), and **e** 90th percentile (K_{ep})

provide results that are often difficult to interpret physiologically [32]. Of note, no statistically significant correlation for K_{ep} or K^{trans} had been found between groups for the PD-L1 TPS threshold of 1%.

PD-L1 expression status is necessary to determine whether a patient should receive immunotherapy as first- or second-line treatment. The 1% threshold establishes eligibility for ICIs, while the 50% threshold identifies patients who benefit most from first-line monotherapy with ICIs targeting the PD-1/PD-L1 axis. For PD-L1 < 50%, combination therapies with ICIs and chemotherapy are preferred to achieve faster responses. This makes the 50% threshold particularly relevant as it provides patient stratification for tailored treatment.

We performed inter-reader agreement analysis to assess the reproducibility of pharmacokinetic features to variations in segmentation. Semi-automatic and manual approaches allowed for greater variability in tumor delineation. Using a high CCC threshold (CCC > 0.85), we conservatively identified median K^{trans} and K_{ep} measures as highly reproducible, further supported by consistent results from mean tumor-wise analysis, reinforcing their reliability as robust imaging biomarkers.

The TWIST sequence accelerates DCE-MRI protocols which are better tolerated by patients with breathing difficulties, such as patients with lung cancer. Our secondary endpoint was to determine a suitable Tofts model configuration for this specific sequence, in terms of model type,

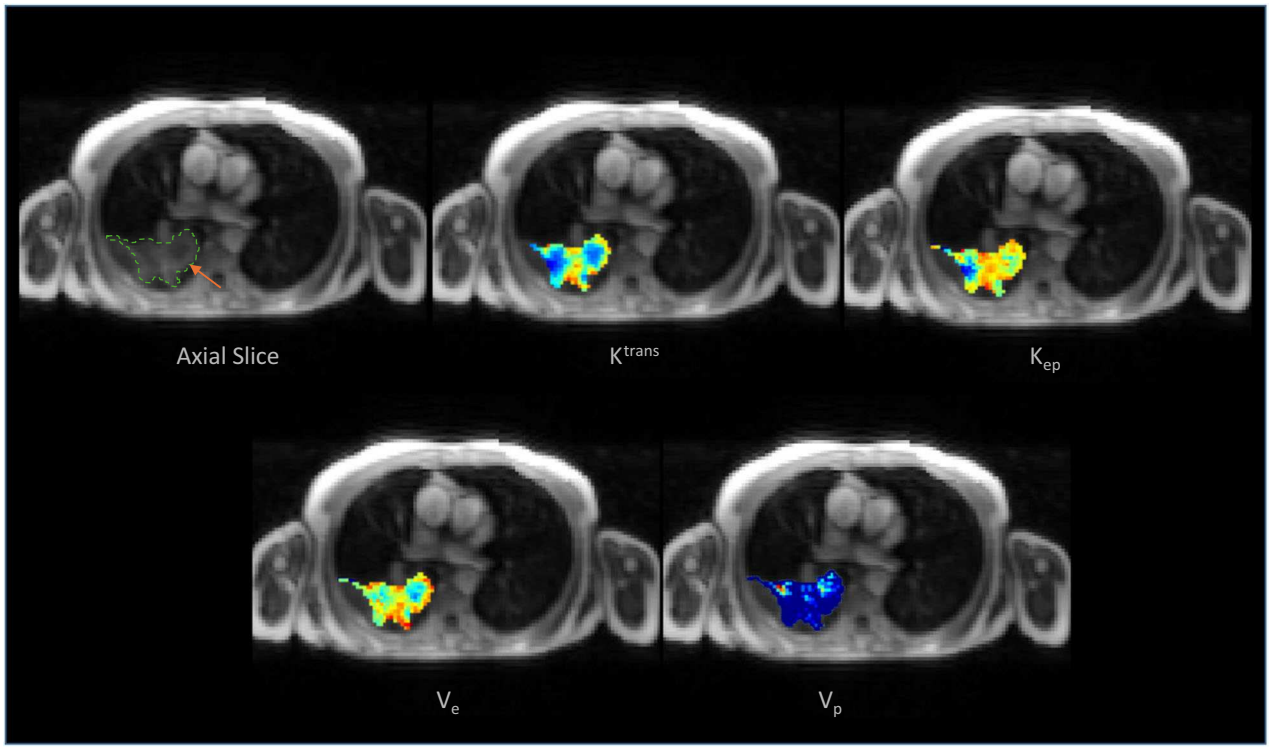


Fig. 4 Illustration of a tumor-focalized DCE-MR axial slice selected from an example patient, along with the corresponding extended Tofts parametric maps extracted using Georgiou arterial input function and peak gradient bolus arrival time estimation method

AIF, and BAT estimation method. Bicompartmental pharmacokinetic models describe the contrast agent dynamics as the interaction between two compartments—vascular space and EES. The key difference between TM and ETM is that the latter extends the standard Tofts model by including V_p in the fit equation, which is particularly relevant in tissues like the lung parenchyma, where the high density of blood vessels can influence contrast agent dynamics.

The AIF, which refers to the concentration of the contrast medium in an artery over time, is a critical input for pharmacokinetic models [38] and can be subject-specific or population-based. We tested population-based AIF because the acquisitions were tumor-focalized, making subject-specific evaluation not feasible. Furthermore, the TWIST protocol, being anisotropic in time, reduces the accuracy of the estimation of subject-specific AIF, as it requires fixed high temporal resolution.

BAT represents the time taken for the contrast medium to reach the target vessel after intravenous injection [39]. Ignoring this parameter can impair pharmacokinetic fit quality [40]. While the Quantitative Imaging Biomarkers Alliance (QIBA) recommends correcting for this delay in the AIF, estimating BAT can be challenging in noise-prone short-duration anisotropically spaced TICs [41]. Hence, we included the delay as an additional parameter in the pharmacokinetic model.

Our analysis revealed that the ETM using either the Georgiou or Parker AIF with PG BAT estimation may be better suited for temporally anisotropic TWIST protocols ($R^2 \sim 0.79$). Further studies may benefit from these results, integrating them with concurrent literature, to ease the analysis pipeline for DCE sequences in the lung cancer setting.

This study, given its preliminary and exploratory nature, has several limitations. First, it is a monocentric study with a relatively small sample size. As a result, the findings may not be fully representative of a larger population and require external validation with data obtained from other centers to ensure their generalizability and reliability. Second, the low availability of lung MRI limits its accessibility for widespread clinical use. However, DCE may be a promising sequence for evaluating the intrinsic properties of tumors, also in association with other MRI sequences. MRI can be repeated regularly, even during therapy, without the use of ionizing radiation; furthermore, this DCE-MRI protocol can be performed in short scanning times, thus it can be easily incorporated into MR exams. Third, the conservative inter-reader agreement analysis is simply indicative but can yield false negatives and requires rigorous validation on a larger population. Lastly, the diagnostic accuracy of K_{ep} and K^{trans} values in

distinguishing between PD-L1 hypoexpression and hyperexpression was moderate, suggesting their potential utility, though not definitive. Future studies should aim to include larger, multicentric cohorts with standardized protocols to confirm these findings.

Conclusions

Quantitative DCE-MRI parameters are potential imaging biomarkers for non-invasively stratifying PD-L1 hyperexpression in NSCLC. We highlight a methodology for choosing among different pharmacokinetic model combinations and identify the most appropriate configuration for temporally anisotropic DCE-MRI sequences.

Abbreviations

AIF	Arterial input function
BAT	Bolus arrival time
CCC	Concordance correlation coefficient
DCE	Dynamic contrast-enhanced
DCE-MRI	Dynamic contrast-enhanced magnetic resonance imaging
EGFR	Epidermal growth factor receptor
ETM	Extended Tofts model
ICI	Immune checkpoint inhibitor
LL	Linear-linear
LQ	Linear-quadratic
NCCN	National Comprehensive Cancer Network
NSCLC	Non-small cell lung cancer
PD-L1	Programmed death-ligand 1
PG	Peak-gradient
QIBA	Quantitative Imaging Biomarkers Alliance
ROC-AUC	Receiver operating characteristics area under the curve
SD	Standard deviation
SM	Supplementary materials
TCC	Time-concentration curve
TIC	Time-signal intensity curve
TM	Standard Tofts model
TPS	Tumor proportion score
TWIST	Time-resolved angiography with interleaved stochastic trajectories
VEGF	Vascular endothelial growth factor
VIBE	Volumetric interpolated breath-hold examination

Supplementary information

The online version contains supplementary material available at https://doi.org/10.1007/s00330-025-11524-1.

Funding

This study was funded by an institutional grant (no. 20190049910) from Fondazione IRCCS Policlinico San Matteo titled "Magnetic Resonance as a specific tool to dissect microenvironment in proliferative lung disease." Open access funding provided by Università degli Studi di Pavia within the CRUI-CARE Agreement.

Compliance with ethical standards

Guarantor

The scientific guarantor of this publication is Prof. Lorenzo Preda, Dept. of Clinical, Surgical, Diagnostic, and Pediatric Sciences, University of Pavia; Radiology Institute, Policlinico San Matteo; lorenzo.preda@unipv.it.

Conflict of interest

A.R.F. declares no conflicts of interest related to this manuscript. Outside the submitted work, he has received institutional grants from AstraZeneca, Merck Sharp Dohme, and Hoffmann-La Roche. He discloses receiving consultation fees from AstraZeneca and Radiomics.bio, and honoraria for lectures, presentations, or educational events from AstraZeneca, Hoffmann-La Roche, and Takeda. AstraZeneca and Elekta have also provided support for attending meetings and/or travels. D.Z. reports no conflicts of interest in this study but discloses his employment with Siemens Healthcare s.r.l. All other authors declare that they have no known competing financial interests or personal relationships that could have appeared to influence the work reported in this paper.

Statistics and biometry

No complex statistical methods were necessary for this paper.

Informed consent

Informed consent was obtained from all subjects involved in the study.

Ethical approval

The study was conducted according to the guidelines of the Declaration of Helsinki and approved by the Institutional Ethics Committee of Fondazione IRCCS Policlinico San Matteo (protocol code P_20190113422 approved on February 10, 2021).

Study subjects or cohorts overlap

Not applicable.

Methodology

- Prospective
- Performed at one institution
- Diagnostic or prognostic study

Author details

[1]Diagnostic Imaging and Radiotherapy Unit, Department of Clinical, Surgical, Diagnostic, and Pediatric Sciences, University of Pavia, Pavia, Italy. [2]Radiology Institute, Fondazione IRCCS Policlinico San Matteo, Pavia, Italy. [3]Clinical Department, National Center for Oncological Hadrontherapy (CNAO), Pavia, Italy. [4]UCLA Brain Tumor Imaging Laboratory (BTIL), Center for Computer Vision and Imaging Biomarkers, University of California Los Angeles, Los Angeles, CA, USA. [5]Department of Radiological Sciences, David Geffen School of Medicine, University of California Los Angeles, Los Angeles, CA, USA. [6]Department of Physics, University of Pavia, Pavia, Italy. [7]Istituto Nazionale Di Fisica Nucleare, Sezione Di Pavia, Pavia, Italy. [8]Euler Institute, Università della Svizzera Italiana, Lugano, Switzerland. [9]Siemens Healthcare srl, Milano, Italy. [10]Department of Medical Sciences and Infective Diseases, Unit of Respiratory Diseases, Fondazione IRCCS Policlinico San Matteo, Pavia, Italy. [11]Department of Internal Medicine and Medical Therapeutics, University of Pavia, Pavia, Italy. [12]Department of Medical Oncology, Fondazione IRCCS Policlinico San Matteo, Pavia, Italy. [13]Radiation Oncology, Fondazione IRCCS Policlinico San Matteo, Pavia, Italy. [14]Radiation Oncology, Fondazione IRCCS Istituto Nazionale dei Tumori, Milan, Italy. [15]Department of Oncology, University of Milan, Milan, Italy

Received: 30 September 2024 Revised: 23 January 2025 Accepted: 18 February 2025
Published online: 27 March 2025

References

1. Bray F, Laversanne M, Sung H et al (2024) Global cancer statistics 2022: GLOBOCAN estimates of incidence and mortality worldwide for 36 cancers in 185 countries. CA Cancer J Clin 74:229–263. https://doi.org/10.3322/caac.21834
2. Herbst RS, Soria J-C, Kowanetz M et al (2014) Predictive correlates of response to the anti-PD-L1 antibody MPDL3280A in cancer patients. Nature 515:563–567. https://doi.org/10.1038/nature14011

3. Garon EB, Rizvi NA, Hui R et al (2015) Pembrolizumab for the treatment of non-small-cell lung cancer. N Engl J Med 372:2018–2028. https://doi.org/10.1056/NEJMoa1501824
4. Herbst RS, Baas P, Kim D-W et al (2016) Pembrolizumab versus docetaxel for previously treated, PD-L1-positive, advanced non-small-cell lung cancer (KEYNOTE-010): a randomised controlled trial. Lancet 387:1540–1550. https://doi.org/10.1016/S0140-6736(15)01281-7
5. Malhotra J, Jabbour SK, Aisner J (2017) Current state of immunotherapy for non-small cell lung cancer. Transl Lung Cancer Res 6:196–211. https://doi.org/10.21037/tlcr.2017.03.01
6. Gompelmann D, Sinn K, Brugger J et al (2023) Correlation of PD-L1 expression on tumour cells between diagnostic biopsies and surgical specimens of lung cancer in real life with respect to biopsy techniques and neoadjuvant treatment. J Cancer Res Clin Oncol 149:1747–1754. https://doi.org/10.1007/s00432-022-04080-4
7. Ettinger DS, Wood DE, Aisner DL et al (2022) Non-small cell lung cancer, version 3.2022, NCCN clinical practice guidelines in oncology. J Natl Compr Canc Netw 20:497–530. https://doi.org/10.6004/jnccn.2022.0025
8. European Medicines Agency (2015) Keytruda. Available via https://www.ema.europa.eu/en/medicines/human/EPAR/keytruda. Accessed 21 Jul 2024
9. Reck M, Rodríguez-Abreu D, Robinson AG et al (2021) Five-year outcomes with pembrolizumab versus chemotherapy for metastatic non-small-cell lung cancer with PD-L1 tumor proportion score ≥ 50. J Clin Oncol 39:2339–2349. https://doi.org/10.1200/JCO.21.00174
10. Gompelmann D, Sarova P, Mosleh B et al (2024) PD-L1 assessment in lung cancer biopsies-pitfalls and limitations. Int J Biol Markers 39:3–8. https://doi.org/10.1177/03936155231214273
11. Huang H, Li Z, Xia Y et al (2023) Association between radiomics features of DCE-MRI and CD8+ and CD4+ TILs in advanced gastric cancer. Pathol Oncol Res 29:1611001. https://doi.org/10.3389/pore.2023.1611001
12. Meyer H-J, Höhn AK, Surov A (2021) Relationships between apparent diffusion coefficient (ADC) histogram analysis parameters and PD-L 1-expression in head and neck squamous cell carcinomas: a preliminary study. Radiol Oncol 55:150–157. https://doi.org/10.2478/raon-2021-0005
13. Ochoa-Albiztegui RE, Sevilimedu V, Horvat JV et al (2020) Pharmacokinetic analysis of dynamic contrast-enhanced magnetic resonance imaging at 7T for breast cancer diagnosis and characterization. Cancers (Basel). https://doi.org/10.3390/cancers12123763
14. Liu Z, Yao B, Wen J et al (2024) Voxel-wise mapping of DCE-MRI time-intensity-curve profiles enables visualizing and quantifying hemodynamic heterogeneity in breast lesions. Eur Radiol 34:182–192. https://doi.org/10.1007/s00330-023-10102-7
15. Bortolotto C, Maglia C, Ciuffreda A et al (2020) The growth of non-solid neoplastic lung nodules is associated with low PD L1 expression, irrespective of sampling technique. J Transl Med 18:54. https://doi.org/10.1186/s12967-020-02241-y
16. Marletta S, Fusco N, Munari E et al (2022) Atlas of PD-L1 for pathologists: indications, scores, diagnostic platforms and reporting systems. J Pers Med. https://doi.org/10.3390/jpm12071073
17. Wang C, Ren Q, Qin X, Yu Y (2018) The same modality medical image registration with large deformation and clinical application based on adaptive diffeomorphic multi-resolution demons. BMC Med Imaging 18:21. https://doi.org/10.1186/s12880-018-0267-3
18. Weinmann HJ, Laniado M, Mützel W (1984) Pharmacokinetics of GdDTPA/dimeglumine after intravenous injection into healthy volunteers. Physiol Chem Phys Med NMR 16:167–172
19. Parker GJM, Roberts C, Macdonald A et al (2006) Experimentally-derived functional form for a population-averaged high-temporal-resolution arterial input function for dynamic contrast-enhanced MRI. Magn Reson Med 56:993–1000. https://doi.org/10.1002/mrm.21066
20. Georgiou L, Wilson DJ, Sharma N, Perren TJ, Buckley DL (2019) A functional form for a representative individual arterial input function measured from a population using high temporal resolution DCE MRI. Magn Reson Med 81:1955–1963. https://doi.org/10.1002/mrm.27524
21. Sanvito F, Raymond C, Cho NS et al (2024) Simultaneous quantification of perfusion, permeability, and leakage effects in brain gliomas using dynamic spin-and-gradient-echo echoplanar imaging MRI. Eur Radiol 34:3087–3101. https://doi.org/10.1007/s00330-023-10215-z
22. Gordon Y, Partovi S, Müller-Eschner M et al (2014) Dynamic contrast-enhanced magnetic resonance imaging: fundamentals and application to the evaluation of the peripheral perfusion. Cardiovasc Diagn Ther 4:147–164. https://doi.org/10.3978/j.issn.2223-3652.2014.03.01
23. Sourbron SP, Buckley DL (2011) On the scope and interpretation of the Tofts models for DCE-MRI. Magn Reson Med 66:735–745. https://doi.org/10.1002/mrm.22861
24. Türkbey B, Thomasson D, Pang Y et al (2010) The role of dynamic contrast-enhanced MRI in cancer diagnosis and treatment. Diagn Interv Radiol 16:186–192. https://doi.org/10.4261/1305-3825.DIR.2537-08.1
25. Wang D, Liu S, Fu J et al (2024) Correlation of Ktrans derived from dynamic contrast-enhanced MRI with treatment response and survival in locally advanced NSCLC patients undergoing induction immunochemotherapy and concurrent chemoradiotherapy. J Immunother Cancer. https://doi.org/10.1136/jitc-2023-008574
26. Sridharan N, Salem A, Little RA et al (2024) Measuring repeatability of dynamic contrast-enhanced MRI biomarkers improves evaluation of biological response to radiotherapy in lung cancer. Eur Radiol. https://doi.org/10.1007/s00330-024-10970-7
27. Guo W, Lv B, Yang T et al (2023) Role of dynamic contrast-enhanced magnetic resonance imaging parameters and extracellular volume fraction as predictors of lung cancer subtypes and lymph node status in non-small-cell lung cancer patients. J Cancer 14:3108–3116. https://doi.org/10.7150/jca.88367
28. Zou M, Zhang B, Shi L, Mao H, Huang Y, Zhao Z (2024) Correlation of MRI quantitative perfusion parameters with EGFR, VEGF and EGFR gene mutations in non-small cell cancer. Sci Rep 14:4447. https://doi.org/10.1038/s41598-024-55033-5
29. Klein D (2018) The tumor vascular endothelium as decision maker in cancer therapy. Front Oncol 8:367. https://doi.org/10.3389/fonc.2018.00367
30. O'Byrne KJ, Koukourakis MI, Giatromanolaki A et al (2000) Vascular endothelial growth factor, platelet-derived endothelial cell growth factor and angiogenesis in non-small-cell lung cancer. Br J Cancer 82:1427–1432. https://doi.org/10.1054/bjoc.1999.1129
31. Essig M, Shiroishi MS, Nguyen TB et al (2013) Perfusion MRI: the five most frequently asked technical questions. AJR Am J Roentgenol 200:24–34. https://doi.org/10.2214/AJR.12.9543
32. Cuenod CA, Balvay D (2013) Perfusion and vascular permeability: basic concepts and measurement in DCE-CT and DCE-MRI. Diagn Interv Imaging 94:1187–1204. https://doi.org/10.1016/j.diii.2013.10.010
33. Meyer HJ, Wienke A, Surov A (2018) Correlation between K_{trans} and microvessel density in different tumors: a meta-analysis. Anticancer Res 38:2945–2950. https://doi.org/10.21873/anticanres.12543
34. Meyer H-J, Höhn AK, Surov A (2021) Associations between dynamic-contrast enhanced MRI and tumor infiltrating lymphocytes and tumor-stroma ratio in head and neck squamous cell cancer. Cancer Imaging 21:60. https://doi.org/10.1186/s40644-021-00429-z
35. Bortolotto C, Stella GM, Messana G et al (2022) Correlation between PD-L1 expression of non-small cell lung cancer and data from IVIM-DWI acquired during magnetic resonance of the thorax: preliminary results. Cancers (Basel). https://doi.org/10.3390/cancers14225634
36. Franz L, Alessandrini L, Calvanese L, Crosetta G, Frigo AC, Marioni G (2021) Angiogenesis, programmed death ligand 1 (PD-L1) and immune microenvironment association in laryngeal carcinoma. Pathology 53:844–851. https://doi.org/10.1016/j.pathol.2021.02.007
37. Lizotte PH, Ivanova EV, Awad MM et al (2016) Multiparametric profiling of non-small-cell lung cancers reveals distinct immunophenotypes. JCI Insight 1:e89014. https://doi.org/10.1172/jci.insight.89014
38. Azahaf M, Haberley M, Betrouni N et al (2016) Impact of arterial input function selection on the accuracy of dynamic contrast-enhanced MRI quantitative analysis for the diagnosis of clinically significant prostate cancer. J Magn Reson Imaging 43:737–749. https://doi.org/10.1002/jmri.25034
39. Bendinger AL, Debus C, Glowa C, Karger CP, Peter J, Storath M (2019) Bolus arrival time estimation in dynamic contrast-enhanced magnetic resonance imaging of small animals based on spline models. Phys Med Biol 64:045003. https://doi.org/10.1088/1361-6560/aafce7
40. Lewis D, Zhu X, Coope DJ et al (2022) Surrogate vascular input function measurements from the superior sagittal sinus are repeatable and provide tissue-validated kinetic parameters in brain DCE-MRI. Sci Rep 12:8737. https://doi.org/10.1038/s41598-022-12582-x

41. Shukla-Dave A, Obuchowski NA, Chenevert TL et al (2019) Quantitative imaging biomarkers alliance (QIBA) recommendations for improved precision of DWI and DCE-MRI derived biomarkers in multicenter oncology trials. J Magn Reson Imaging 49:e101–e121. https://doi.org/10.1002/jmri.26518

Publisher's Note

Springer Nature remains neutral with regard to jurisdictional claims in published maps and institutional affiliations.